

# Global Behavior of the Radial Orbit Instability

Paul A. Lanzel

Eric I. Barnes — Faculty Advisor

*Department of Physics, University of Wisconsin — La Crosse, La Crosse, WI 54601*

lanzel.paul@gmail.com

barnes.eric@uwlax.edu

## ABSTRACT

A variety of evidence points to the existence of dark matter in the universe. As it is not directly observable with conventional astronomical techniques, we must rely on computer models to guide our understanding. We have created a suite of such models in order to observe and explain a specific behavior common to models of dark matter systems called the radial orbit instability (ROI). This instability changes self-gravitating systems from spherical to non-spherical shapes, with corresponding alterations to density and velocity distributions. The initial conditions of our models span a parameter space that is relevant to the radial orbit instability; we control the initial dynamical temperature, density profile, and velocity anisotropy in our models. We have found that in dynamically hot and warm systems, the radial orbit instability will be triggered if the initial velocity anisotropy is high enough. The exact amount of anisotropy required varies somewhat for different initial density profiles. Dynamically cold systems behave somewhat differently, but in general, less initial anisotropy is required to initiate the ROI as compared to hot and warm systems.

## 1. Introduction

Astronomy and astrophysics are, in some sense, more closely related to archaeology than physics. Like an archaeologist relying on the remnants of eras past, astrophysicists rarely have the luxury of making direct measurements of their subjects and often depend upon inference and indirect means of supporting hypotheses. This is certainly true for those of us who are interested in galaxies. Galaxies are vast collections of stars, gas, and dust of which the NASA Great Observatory space telescopes (Hubble, Chandra, Spitzer, and Compton) continue to provide breathtaking images.

Astrophysicists continue to search for a fundamental picture of how galaxies form and evolve. Since an analogous system of understanding is already largely in place for stars, one might expect that since galaxies are mainly composed of stars, this task would be straightforward. What makes studying galaxies interesting is that the stars are not the most important component of galaxies, at least from the viewpoint of gravity. An analogy to icebergs is often used to clarify our current understanding of galaxies. Stars, gas, and dust (collectively referred to as visible matter since they can produce or absorb light) are the ice that lies above the surface of the ocean. However, given the structure and behavior of this visible ice, we can infer that below the surface is a large, unseen mass. In a galactic context, this mass has become known as dark matter since it does not interact with light in any way. Dark matter neither emits, absorbs, nor reflects light. Given that astronomers mainly use light to detect and study objects in the universe, one is certainly justified in asking, “How can we know there is any dark matter at all?”.

The motions of stars and gas in spiral galaxies indicate that individual galaxies are enveloped in dark matter “halos” with roughly 10 to 100 times the total mass of the galaxy’s stars (for example, see Salpeter 1978; Rubin 1979; Sancisi & Allen 1979). Additionally, models of the gravitational lensing of light from distant quasars by individual galaxies require similarly large amounts of dark matter to match observations (Schechter & Wambsganss 2004; Ferreras *et al.* 2005). On a very different scale, the motions of individual galaxies within galaxy clusters, which contain hundreds to thousands of galaxies, are also difficult to explain without including large amounts of dark matter throughout the clusters (Zwicky 1937). Recently, detailed observations of the cosmic microwave background (CMB) have been analyzed (Spergel *et al.* 2007). The model of the universe that best explains the distribution of CMB light requires that the bulk of the mass in the universe is not baryonic, or “normal”, matter. Specifically, this model universe is composed of matter ( $\approx 25\%$  of the total mass-energy budget) and dark energy (the remaining 75% of the budget). While dark energy is a fascinating topic, we will not discuss it further here. Rather, we will focus on the dark matter component, which comprises about 80-90% of the total mass in the universe.

In an effort to understand how dark matter behaves and shapes the formation of galaxies in the universe, astrophysicists have turned to computer models that evolve large numbers of massive particles under the influence of gravity alone. Such models are referred to as  $N$ -body models, where  $N$  is typically much larger than 10. The large number of particles makes the models approximately collisionless. That is, the motions of the particles are determined by the global distribution of matter in the system, not individual encounters with near-by neighbor particles. Simulations of  $N$ -body systems are tools for analyzing the physics behind self-gravitating, collisionless systems of massive particles. We are particularly interested in the physics of models that undergo a collapse phase during their evolution and how collapse shapes a models’ long-term behavior.

We have created sets of  $N$ -body simulations to investigate a process that is thought to

be important to the formation of dark matter halos, the radial orbit instability (ROI). We provide a brief summary of previous works that deal with the ROI (Polyachenko & Shukhman 1981; van Albada 1982; Merritt & Aguilar 1985; Palmer & Papaloizou 1987; Huss, Jain, & Steinmetz 1999). The ROI is most evident when the particles in an initially spherical system have a high degree of radial motion. Any slight bar-like concentration of particles leads to torques that pull neighboring particles into the bar, increasing the torque strength and perpetuating the instability. The ROI drives such a system towards a prolate spheroidal or triaxial shape. This rearrangement of mass can greatly influence the density distribution and evolution of the halo. Our specific goal is to determine and describe the factors that instigate and drive the ROI. To this end, we focus on models with varying degrees of initial velocity anisotropy; large amounts of radial velocity anisotropy should lead to the ROI, while isotropic velocity distributions should not.

In Section 2, we detail the various initial conditions that influence our simulations and the methods used to evolve our models. Section 3 contains our results as they pertain to the global factors influencing the onset of the ROI. We summarize our work and conclusions in § 4.

## 2. Methods & Testing

### 2.1. Initial Conditions

The initial conditions for our models are the control parameters for our investigation. Density profiles, velocity distributions, system mass, and system size are all determined before any simulation begins. Our choices for each are designed to span a wide range of the parameter space relevant to the ROI. Each model discussed here is made up of  $N = 10^4$  particles, has a total mass  $M = 1$  (in dimensionless code units), and an outer spherical edge with radius  $R = 1$  (again, in code units).

We have chosen three initial density distributions to investigate. Models are given uniform ( $\rho = \rho_0$ ), cuspy ( $\rho \propto r^{-1}$ ), or Gaussian ( $\rho \propto e^{-r^2}$ ) radial density profiles. Particle positions are chosen randomly inside the spherical system so that the appropriate distribution is achieved using a Metropolis-like approach. With the particle positions set, the potential energy  $W$  of the model is determined.

To complete the initial conditions, we set the velocity of each particle. We do this in two steps; (1) set a scale speed for the system that will determine each particle's speed and (2) choose directions for each vector. The virial theorem is used to relate the total kinetic energy  $T$  of a system to its total potential energy  $|W|$ . Specifically, any gravitationally bound system in virial equilibrium has  $T = |W|/2$ . For each model, we choose an initial virial ratio

value  $Q_0$ , defined by

$$Q_0 = \frac{2T}{|W|}. \quad (1)$$

In this notation, the model is in virial equilibrium when  $Q_0 = 1$ . We note that throughout this work, any variable with a subscript ‘0’ denotes an initial value. For a given  $Q_0$  and  $W$ , the value of  $T$  is set. The speed of each particle is chosen so that the average speed for the entire model is  $v_{\text{scale}}$ , where  $T \equiv \frac{1}{2}Mv_{\text{scale}}^2$ . We evolve models with  $Q_0 = 1.0, 0.5, 0.2$ , and  $0.1$  to gauge the impact of this quantity on the ROI. Since models with larger values of  $Q_0$  have more kinetic energy, they are often referred to as dynamically hot, keeping with the kinetic theory definition of temperature. We will refer to models with  $Q_0 = 1.0$  as “hot”,  $Q_0 = 0.5$  and  $0.2$  as “warm”, and  $Q_0 = 0.1$  as “cold”. Changing  $Q_0$  is a simple way to control the strength of the collapse that will occur during a model’s evolution. Cold models should have the strongest collapses as the effect of the system’s gravity will be to immediately pull all particles towards the center. Conversely, the particles in hot models feel a gravitational pull towards the center, but their substantial initial momenta generally delay and weaken the collapse (for  $Q_0 > 1.0$  at least some particles are unbound).

Choosing the directions of each particle’s velocity vector requires some care so that we can accurately control the velocity anisotropy in a model. The velocity anisotropy  $\beta$  for a set of particles is defined by,

$$\beta \equiv 1 - \frac{\sigma_{\text{tan}}^2}{2\sigma_r^2}, \quad (2)$$

where  $\sigma_{\text{tan}}$  and  $\sigma_r$  are, respectively, the tangential and radial velocity dispersions for that set of particles. The tangential dispersion has two components, one for polar velocities and one for azimuthal velocities;  $\sigma_{\text{tan}}^2 = \sigma_\theta^2 + \sigma_\phi^2$ . Note that the dispersion here is referring to the quantity  $\sigma^2 = \langle v^2 \rangle - \langle v \rangle^2$ , where the angle brackets indicate averages. The velocity dispersion is most easily thought of as a measure of the spread of the velocities around their mean for a set of particles (in our work, particles within concentric spherical shells).  $\beta$  may have a constant value throughout an entire system, or it may be a function of position within a system. We will briefly discuss a few examples of constant  $\beta$  before continuing on to anisotropy distributions.

In a model where the velocity distribution is isotropic,  $\beta = 0$  throughout the system, and a particle’s velocity vector points in a randomly chosen direction. Another way of thinking about isotropic velocities is that  $\sigma_r^2 = \sigma_\theta^2 = \sigma_\phi^2$ ; the amount of random motion in every direction is the same. This situation also points to the reason for the factor of 2 in the denominator of Equation 2 :  $\beta = 0$  when  $\sigma_{\text{tan}}^2 = 2\sigma_r^2$ , as in this case. A model with a completely radially anisotropic velocity distribution,  $\beta = 1$  everywhere in the model, is constrained to have velocity vectors that are directed towards or away from the center of the system.

We use a flexible anisotropy profile  $\beta(r)$  (Barnes *et al.* 2007) to control the amount of radial velocity anisotropy in our models. Depending on their radial distance, some particles

will be set on orbits that are more radially-oriented than others. This flexible  $\beta(r)$  is given by

$$\beta(r) = \frac{1}{2}(\beta_{\text{high}} - \beta_{\text{low}})[1 + \tanh(m \log r/r_a)] + \beta_{\text{low}}, \quad (3)$$

where  $\beta_{\text{low}}$  is the anisotropy value at the center of the system  $r = 0$ ,  $\beta_{\text{high}}$  is the anisotropy value at the edge of the system  $r = R = 1$ ,  $m$  controls the transition between these values, and  $r_a$  is the anisotropy radius at which  $\beta = 0.5$ . For the models presented here,  $\beta_{\text{low}} = 0$  and  $\beta_{\text{high}} = 1$ . We use a slope  $m = 7$  to give a relatively localized transition between the low and high  $\beta$  values; smaller  $m$  would force the transition to occur over a wider range of  $r$ , while larger  $m$  would make the transition more step-like. Defining  $\beta$  as a function of  $r$  gives us the ability to control the quantity and location of the mass that is initially isotropic or radially anisotropic. In general, the central regions of our models have isotropic velocity distributions with a transition to radially anisotropic distributions near the edges. We use  $r_a$  as the main control over the anisotropy of a model; small values of  $r_a$  drive more particles to be on radially anisotropic orbits, while larger values force the system to be more isotropic (in terms of velocity). Our models include systems with  $r_a = 0.1$  to 1.2 in steps of 0.1.

The general method for assigning velocity vectors to fit a given  $\beta$  profile is as follows. For a given particle, a  $\beta$  value is calculated from Equation 3. This value is transformed into an “opening angle” for the velocity vector. Imagine two cones with apexes at the particle and symmetry axes along the radial direction; one cone opens outward and one cone opens towards the center of the halo. When  $\beta = 0$ , the angle will be  $\pi$  and the velocity vector will be randomly assigned a direction within  $4\pi$  steradians; this will give an isotropic system. When  $\beta = 1$ , the angle will be zero and the velocity vector will be completely radial. For values of  $\beta$  between zero and one, the opening angle varies linearly between these extremes.

At this point, we have specified the positions and velocities of each of our  $N$  particles. Note that the important control parameters are the density profile  $\rho(r)$ , the initial virial ratio  $Q_0$ , and the anisotropy radius  $r_a$ . We now briefly discuss how the particles are evolved in time and analyzed.

## 2.2. Evolution & Analysis

Models are evolved using the direct  $N$ -body integration code NBODY2; for further details on NBODY2 algorithms, see Aarseth (2001). In the code, the gravitational force between any two particles  $i$  and  $j$  is given by,

$$\vec{F}_{ij} = -G \frac{m_i m_j}{(r_{ij}^2 + \epsilon^2)^{3/2}} (\vec{r}_i - \vec{r}_j) \quad (4)$$

where  $G = 1$  in code units,  $m_i$  and  $m_j$  are the masses of the particles,  $\epsilon$  is the “softening” length, and  $r_{ij}$  is the distance between particles. Note that just as  $G$  is dimensionless in code units, so are distances like  $\epsilon$  and  $r_{ij}$ . Basically, these dimensionless distances represent

measurements with respect to the initial radius of the system. It can be seen in Equation 4 that without the inclusion of the softening term  $\epsilon$ , the gravitational force between two particles approaches infinity as the distance  $r$  between the two particles approaches zero. This would, in effect, represent a collisional system which deviates from the seemingly collisionless nature of dark matter. By including the softening value, we set a maximum gravitational force between any two particles and do not allow it to go to infinity. The particles are then essentially collisionless and yet we must take care that the softening is small enough to retain the force’s Newtonian character overall. We have tested the collisional nature of our simulations by varying the values for  $\epsilon$  from  $\epsilon = 5 \times 10^{-4}$  to  $\epsilon = 5 \times 10^{-2}$ , similar to the range suggested by Power *et al.* (2003). Differences between evolutions having  $\epsilon$  within this range are minimal. The models presented here use the smallest softening value,  $\epsilon = 5 \times 10^{-4}$ . As a further test of the collisionality of our models, we have also evolved models with particles of different masses. If collisions play a significant role in the evolution, particles with larger masses should “sink” to the center of the system, as collisions with lighter particles should rob them of kinetic energy. We find no evidence of mass segregation in any of these tests, assuring us that our models avoid undesirable two-body collision effects and accurately simulate Newtonian gravity. Evolutions of models with different numbers of particles ( $N = 5 \times 10^3$  and  $N = 10^4$ ) have also been conducted. Again, the differences between the various models are minimal, but we have opted to use  $N = 10^4$  for increased resolution. Our choices of  $\epsilon$  and  $N$  allow us to perform the large number of simulations necessary to investigate our rather large parameter space while adhering to the collisionless condition required.

The initial density profile determines the crossing time,  $t_{cross}$ , which is used as the time interval for NBODY2. Most systems evolve for about 20  $t_{cross}$ ; all systems come to virial equilibrium during their evolutions and most reach mechanical equilibrium as well. Depending on the nature of the collapse, some halos that reach virial equilibrium have approximately 5% of their total mass that continues to expand throughout the evolution. During an evolution, NBODY2 regularly produces data that is collected as a “snapshot”. These snapshots are measurements of particle numbers, positions, velocities, energies, collision data and more. These time-sequence measurements are then used in the analysis of system shape, density, velocity dispersion, and anisotropy for the systems.

Systemic axis ratios are calculated throughout an evolution using the moment of inertia tensor of the innermost 95% of the mass. We exclude the outermost 5% as it is sometimes not in mechanical equilibrium. These axis ratios are reported as  $\frac{b}{a}$  and  $\frac{c}{a}$ , where  $a$ ,  $b$ , and  $c$  are the lengths of the long, intermediate, and short axes of a system. Initially,  $\frac{b}{a}$  and  $\frac{c}{a}$  are both very close to 1, as one would expect for a spherical system. There are four system shapes that we differentiate. If  $\frac{b}{a} \approx \frac{c}{a} > 0.8$ , we consider the system to be spherical. We chose this definition largely because systems fulfilling this criteria look spherical, by eye. We consider systems oblate spheroidal when  $\frac{b}{a} \gtrsim 0.8$  and  $\frac{c}{a} \lesssim 0.8$ . If the axis ratios of a system are  $\frac{b}{a} \approx \frac{c}{a} < 0.8$ , we refer to it as prolate spheroidal. Finally, triaxial systems are those that

have  $\frac{b}{a} \neq \frac{c}{a}$ ,  $\frac{b}{a} < 0.8$ , and  $\frac{c}{a} < 0.8$ . In general, to determine whether or not the ROI has occurred, we need only observe whether or not a system has evolved from a spherical shape to one of the other three. Given that  $\frac{c}{a}$  compares the shortest axis to the longest, we use its minimum value during an evolution to gauge the maximum strength of the ROI.

We divide systems of particles into concentric spherical shells, each containing 5% of the total mass (typically 500 particles). This gives us a radial profile of quantities like density and velocity distributions. The inner/outer radii and average densities of the shells are saved. The velocity dispersions and  $\beta$ -values for the particles in each shell are also calculated throughout the evolution. We quantify the velocity anisotropy of our models using the fractions of particles that are on isotropic, tangentially anisotropic, and radially anisotropic orbits. The mass within a shell is considered to be isotropic if  $-1.0 < \beta < 0.5$ , tangentially anisotropic if  $\beta < -1.0$ , and radially anisotropic if  $\beta > 0.5$ . For example, if a given model has 5 shells that are isotropic, 10 shells that are radially anisotropic, and 5 shells that are tangentially anisotropic, we would assign an isotropic mass fraction  $\mu_i = 0.25$ , a radial mass fraction  $\mu_r = 0.50$ , and a tangential mass fraction  $\mu_t = 0.25$ . While  $\mu_r$  and  $\mu_t$  can be combined to account for the total anisotropic mass fraction  $\mu_a$ , where  $\mu_i + \mu_a = 1$ , we distinguish the two types of anisotropic motion to quantify their behaviors and isolate their impacts during the ROI.

Rather than using  $r_a$ , which does not have a simple physical interpretation, we use these mass fractions to quantify the anisotropy of our models. Specifically, we use the initial radial mass fraction  $\mu_{r,0}$  as one of our parameter space dimensions (initial density profile and  $Q_0$  are the other two). It should be mentioned that  $\mu_r$  has a monotonic, one-to-one correlation with the global anisotropy parameter  $A \equiv 2T_r/T_t$ , where  $T_r$  is the kinetic energy of radial motions and  $T_t$  is the kinetic energy in tangential motions. This global quantity has been used as a predictor of ROI by Polyachenko & Shukhman (1981); Merritt & Aguilar (1985); Barnes *et al.* (1986); Bellovary *et al.* (2008). The benefit of using  $\mu_{r,0}$  rather than  $A_0$  is that  $\mu_{r,0}$  has a more straightforward interpretation. We point out that the work presented here is a much more thorough examination of parameter space than was attempted in any previous work. We report on the correlations between our parameter space dimensions in the next section.

### 3. Results

We have found that both  $Q_0$  and  $\mu_{r,0}$  influence the onset and evolution of the ROI. First, we look at how the ROI, in hot and warm systems, is affected by increasing  $\mu_{r,0}$ . Second, we find that cold systems have an initial density profile dependence which influences the ROI. The axis ratios that are discussed in this section are the values of  $\frac{b}{a}$  and  $\frac{c}{a}$  when  $\frac{c}{a}$  is at its minimum for the evolution; *i.e.*, the maximum departure from spherical symmetry.

### 3.1. Hot & Warm Models

For hot and warm systems ( $Q_0 \geq 0.2$ ), we find that systems with small  $\mu_{r,0}$  retain spherical shapes, while larger values of  $\mu_{r,0}$  lead to prolate and triaxial systems. This behavior is independent of initial density profile. Our results show that there is a threshold value for  $\mu_{r,0}$  beyond which our models no longer remain spherical; they will evolve into prolate spheroidal or triaxial shapes.

When comparing systems with different initial density profiles, there are three different  $\mu_{r,0}$  threshold values that are largely independent of  $Q_0$ . An example of this behavior is shown in Figure 1 for a model with  $Q_0 = 0.5$  and an initially Gaussian density profile (we

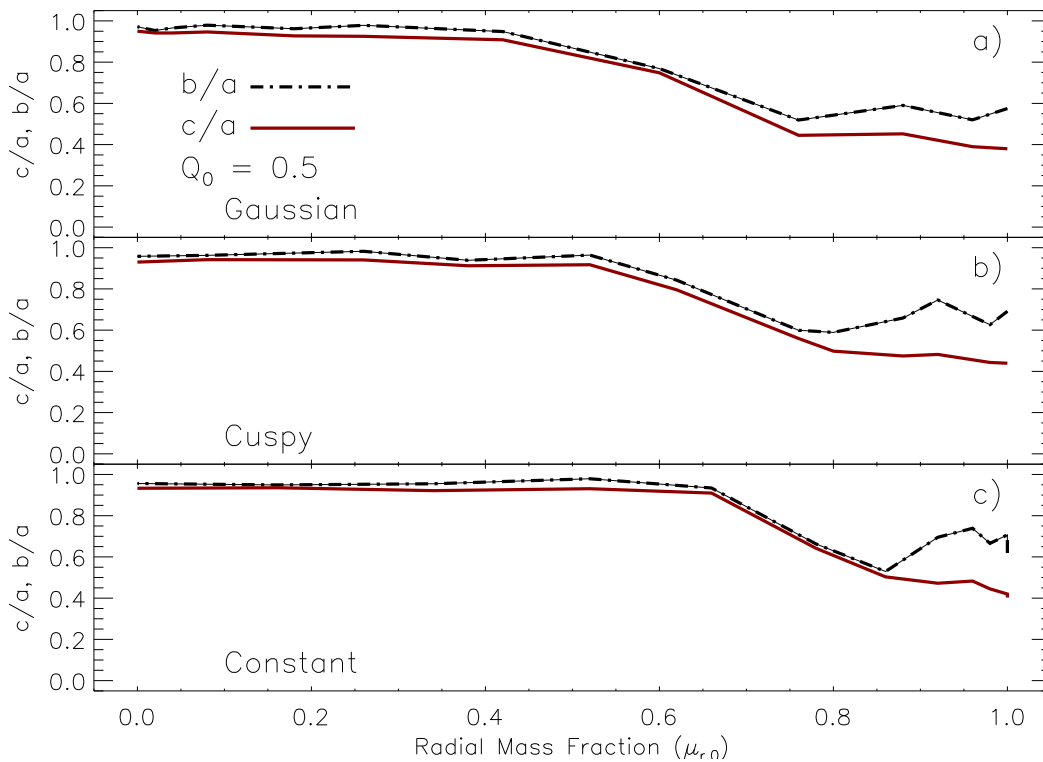


Fig. 1.— Panels a, b, and c show the minimum axis ratios for the innermost 95% of mass as functions of  $\mu_{r,0}$  for models with constant, cuspy, and Gaussian initial density profiles, respectively. The dot-dash line represents the minimum  $\frac{b}{a}$  axis ratio and the solid line represents the minimum  $\frac{c}{a}$  axis ratio. While these specific correlations derive from models with  $Q_0 = 0.5$ , we find nearly identical behaviors in all models with  $Q_0 \geq 0.2$ . The spherical-to-non-spherical anisotropy threshold values for the three initial density cases are;  $\mu_{r,0} = 0.42$  for Gaussian models,  $\mu_{r,0} = 0.52$  for cuspy models, and  $\mu_{r,0} = 0.66$  for constant density models.

note that this curve is nearly identical for the  $Q_0 = 1.0$  and  $0.2$  models). When  $\mu_{r,0} \leq 0.42$ , Gaussian models remain approximately spherical. As  $\mu_{r,0}$  increases ( $0.42 \leq \mu_{r,0} \leq 0.76$ ), Gaussian models become prolate spheroidal at the height of the ROI. For models with  $\mu_{r,0} \geq 0.76$ , the systems become more triaxial as  $\mu_{r,0}$  increases; the minimum  $\frac{c}{a}$  value continues to decline but the minimum  $\frac{b}{a}$  value begins to rise. We see a very similar pattern for all three initial density profiles when  $Q_0 \geq 0.2$ . Initially cuspy and constant density models have spherical-to-non-spherical threshold values of  $\mu_{r,0} = 0.52$  and  $\mu_{r,0} = 0.66$ , respectively.

We explain the observed increase in threshold value as follows. Each density profile (constant, cuspy, and Gaussian) provides a different concentration of particles near the centers of systems. Constant density models will have the fewest particles near the center and Gaussian models will have the most. Any bar-like structure that appears near the center of a system with a high central density can easily ensnare neighboring particles and grow stronger. A similar structure in a system with a relatively lower central density can only grow stronger if particles from the outer regions of the system come into the center where they can be trapped by the growing bar. Because of the imposed shape of the initial anisotropy profile, larger values of  $\mu_{r,0}$  correspond to systems with smaller isotropic central regions and larger regions of radially anisotropic mass extending inward from the edge. Systems with lower central density can fall prey to the ROI only if there are enough outer region particles coming into the center, and that requires a larger  $\mu_{r,0}$ .

### 3.2. Cold Models

Cold models ( $Q_0 = 0.1$ ) behave somewhat differently than their warm and hot counterparts. The combination of small initial particle velocities and the gravitational pull towards the center of the system greatly increases the number of particles with almost purely radial motion. While this collapsing motion does not initially create high velocity dispersions, particles that have passed through the center of mass quickly create the dispersions needed to initiate the ROI; for more details on cold system collapses related to ROI, see Barnes *et al.* (2009). These delayed, but strong dispersions, lead to an overall increase in the strength of the ROI, but the radial mass fraction  $\mu_{r,0}$  is no longer the primary instigator of the ROI due to the low initial particle velocities.

Figure 2 illustrates the behavior of  $Q_0 = 0.1$  model axis ratios as a function of initial radial mass fraction for each initial density profile. The Gaussian and cuspy models still follow the same basic pattern as those of the warmer models with the exception that their threshold values for  $\mu_{r,0}$  are significantly lower; Gaussian and cuspy models have threshold values of  $\mu_{r,0} = 0.18$  and  $\mu_{r,0} = 0.26$ , respectively. Models with constant density no longer follow the same type of pattern. This is not surprising since many of these cold evolutions lead to large amounts of mass loss (up to  $\approx 35\%$ ) for this initial density profile. The systems that the axis ratios are measuring in these cases are really just “core” remnants of the initial

systems. Again, the ROI will not occur if the bar-like structure near the center cannot grow.

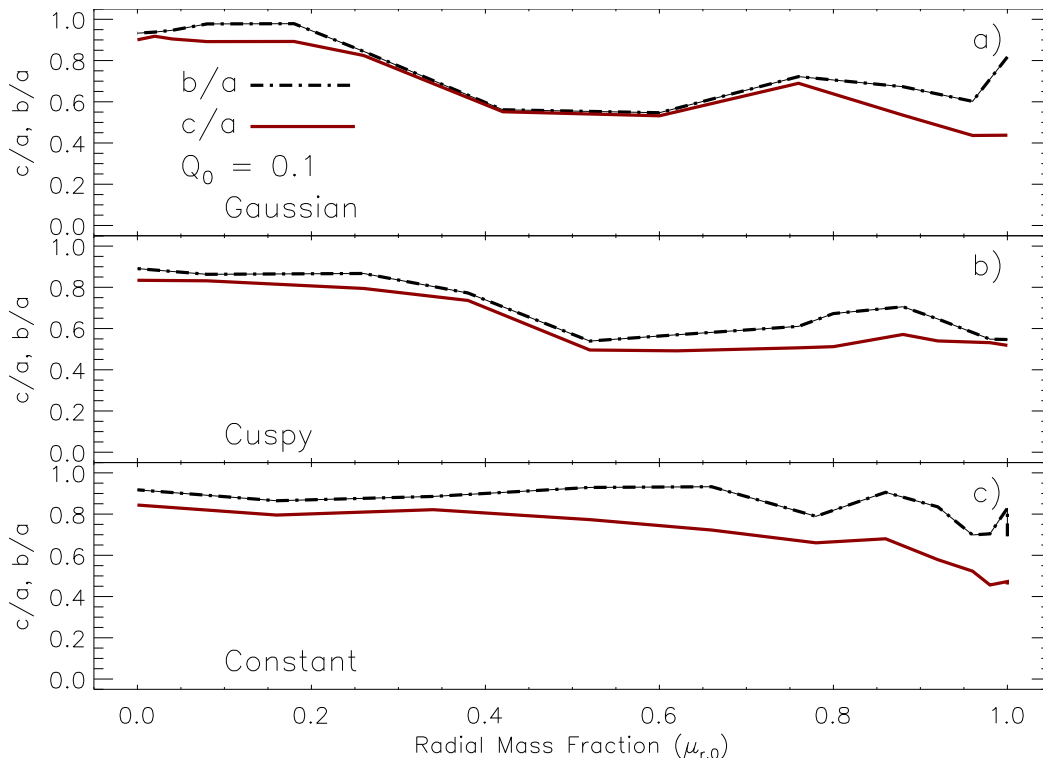


Fig. 2.— As in Figure 1, panels a, b, and c display the minimum axis ratios for the innermost 95% of mass as functions of  $\mu_{r,0}$  but for cold models with  $Q_0 = 0.1$ . From top to bottom, the panels represent models with initially Gaussian, cuspy, and constant density profiles. The dot-dash lines represent the minimum  $\frac{b}{a}$  axis ratios and solid lines represent the minimum  $\frac{c}{a}$  axis ratios. The threshold values for the Gaussian ( $\mu_{r,0} = 0.18$ ) and cuspy models ( $\mu_{r,0} = 0.26$ ) are substantially lower than in warmer models, but the presence of the threshold remains quite clear. Models with initially constant density profiles do not show clear threshold values. The axis ratios instead have moderately non-spherical values for low  $\mu_{r,0}$ , and become somewhat more triaxial as  $\mu_{r,0}$  increases. We suspect this difference in constant density model behavior stems from the significant mass loss that can occur in these models.

#### 4. Summary & Conclusions

In an effort to increase the understanding of the physics involved in dark matter halo formation and evolution, we have created a suite of models with initial conditions designed to explore a parameter space relevant to the radial orbit instability (ROI). The ROI is an important process in dark matter halo evolution as it changes the overall shape of a system, impacting the density and velocity distributions. These are fundamental quantities that are

necessary when comparing the results of simulations to observations.

We create models with different initial density profiles, initial virial ratios  $Q_0$  and initial radial mass fractions  $\mu_{r,0}$ . We explore this parameter space by evolving our models with a well-known computer code that accurately follows the behavior of self-gravitating systems. In particular, we are interested in how the overall shapes of our models (quantified by axis ratios) change during their evolutions. Systems that evolve from spherical to either prolate spheroidal or triaxial shapes indicate the presence of the ROI.

We have identified threshold values of  $\mu_{r,0}$  that separate systems of particles that evolve spherically from those that become non-spherical. Dynamically hot and warm models have similar behaviors, in that a clear transition is visible in terms of  $\mu_{r,0}$  values. Sets of models with each initial density profile show this same behavior, but the specific threshold value changes slightly for each. Models that are dynamically cold react differently than those that are warm. Cold, initially constant density models tend to lose substantial fractions of mass during their evolutions, leaving nearly spherical remnants for almost all values of  $\mu_{r,0}$ . Initially cuspy and Gaussian models again have threshold  $\mu_{r,0}$  values, but the values are much lower than those for the hot and warm models. This is not surprising as the colder initial conditions allow the systems to develop some radial velocity anisotropy through collapse; a smaller amount of initial anisotropy is required to trigger the ROI.

The following chart summarizes how the values for  $\mu_{r,0}$  relate to  $Q_0$ , initial density profile, and the shape of the system when the ROI is at maximum strength. The smaller  $\mu_{r,0}$  number is the threshold value needed to initiate the ROI. Models with smaller values remain spherical. The larger  $\mu_{r,0}$  number defines the break between prolate and triaxial systems, with larger  $\mu_{r,0}$  leading to triaxial shapes. Systems with intermediate values will result in prolate spheroidal systems. See Figure 3 on the following page for a more visual interpretation.

Q	$\rho(r)$	Prolate Spheroidal Range
1.0	constant	$0.66 < \mu_{r,0} < 0.92$
	cuspy	$0.52 < \mu_{r,0} < 0.80$
	Gaussian	$0.42 < \mu_{r,0} < 0.76$
0.5	constant	$0.66 < \mu_{r,0} < 0.86$
	cuspy	$0.52 < \mu_{r,0} < 0.80$
	Gaussian	$0.42 < \mu_{r,0} < 0.76$
0.2	constant	$0.66 < \mu_{r,0} < 0.86$
	cuspy	$0.52 < \mu_{r,0} < 0.80$
	Gaussian	$0.42 < \mu_{r,0} < 0.88$
0.1	constant	...
	cuspy	$0.26 < \mu_{r,0} < 0.62$
	Gaussian	$0.18 < \mu_{r,0} < 0.76$

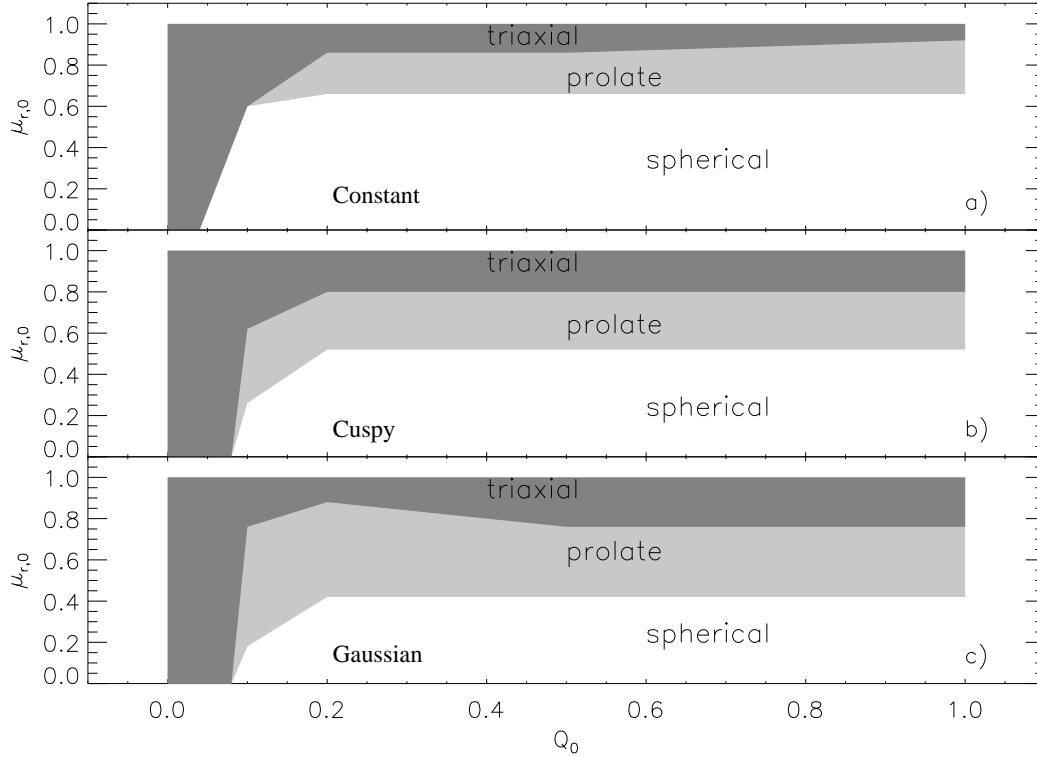


Fig. 3.— The shaded regions in these panels show the boundaries for initial conditions that produce the listed system shapes when the ROI is at its maximum strength. Spherical shapes result from initial conditions in the white areas, prolate shapes result from initial conditions in the light gray areas, and triaxial shapes result from initial conditions in the dark gray areas. Panels a, b, and c represent initially constant, cuspy, and Gaussian density distributions, respectively. In summary, an initially spherical system will evolve into either a prolate or triaxial system if  $\mu_{r,0}$  is high enough. While threshold values for  $\mu_{r,0}$  are relatively constant for  $Q_0 \geq 0.2$ ,  $\mu_{r,0}$  has less of an effect as  $Q_0 \lesssim 0.1$ .

The authors gratefully acknowledge support from NASA Astrophysics Theory Program grant NNX07AG86G.

## REFERENCES

- Aarseth, S. J. 2001, *New Astron.*, **6**, 277-291.
- Barnes, J., Goodman, J., Hut, P. 1986, *Astrophys. J.*, **300**, 112-131.
- Barnes, E. I., Williams, L. L. R., Babul, A., Dalcanton, J. J. 2007, *Astrophys. J.*, **654**, 814-824.
- Barnes, E. I., Lanzel, P., Williams, L. L. R. 2009, in preparation.
- Bellovary, J. M., Dalcanton, J. J., Babul, A., Quinn, T. R., Maas, R. W., Austin, C. G., Williams, L. L. R., Barnes, E. I. 2008, *Astrophys. J.*, **685**, 739-751.
- Ferreras, I., Saha, P., Williams, L. L. R. 2005, *Astrophys. J. Lett.*, **623**, 5-8.
- Huss, A., Jain, B., Steinmetz, M. 1999, *Astrophys. J.*, **517**, 64-69.
- Merritt, D., Aguilar, L. A. 1985, *Mon. Not. Roy. Ast. Soc.*, **217**, 787-804.
- Palmer, P. L., Papaloizou, J. 1987, *Mon. Not. Roy. Ast. Soc.*, **224**, 1043-1053.
- Polyachenko, V. L., Shukhman, I. G. 1981, *Soviet Astron.*, **25**, 533.
- Rubin, V. C. 1979, *Comments Astrophys.*, **8**, 79-88.
- Salpeter, E. E. 1978, in *IAU Symp. 77, Structure and Properties of Nearby Galaxies*, ed. E. M. Berkhuijsen & R. Wielebinski (Dordrecht:Reidel), 23-26.
- Sancisi, R., Allen, R. J. 1979, *Astron. & Astrophys.*, **74**, 73-84.
- Schechter, P. L., Wambsganss, J. 2004, in *IAU Symp. 220, Dark Matter in Galaxies*, ed. S. D. Ryder, D. J. Pisano, M. A. Walker, and K. C. Freeman (San Francisco: Astronomical Society of the Pacific), 103.
- Spiegel, D. N., Bean, R., Dore, O., Nolta, M.R., Bennett, C.L., Dunkley, J., Hinshaw, G., Jarosik, N., Komatsu, E., Page, L., Peiris, H.B., Verde, L., Halpern, M., Hill, R.S., Kogut, A., Limon, M., Meyer, S.S., Odegard, N., Tucker, G.S., Weiland, J.L., Wollack, E., Wright, E.L. 2007, *Astrophys. J. Supp.*, **170**, 377-408.
- van Albada, T. S. 1982, *Mon. Not. Roy. Ast. Soc.*, **201**, 939-955.
- Zwicky, F. 1937, *Astrophys. J.*, **86**, 217.

**Key words:** Astrophysics, computer simulation, dark matter, Newtonian gravitation, orbit stability, virial theorem